

Link between spin fluctuations and electron pairing in copper oxide superconductors

K. Jin^{1,2}, N. P. Butch^{1,2}, K. Kirshenbaum^{1,2}, J. Paglione^{1,2} & R. L. Greene^{1,2}

Although it is generally accepted that superconductivity is unconventional in the high-transition-temperature copper oxides, the relative importance of phenomena such as spin and charge (stripe) order, superconductivity fluctuations, proximity to a Mott insulator, a pseudogap phase and quantum criticality are still a matter of debate¹. In electron-doped copper oxides, the absence of an anomalous pseudogap phase in the underdoped region of the phase diagram² and weaker electron correlations^{3,4} suggest that Mott physics and other unidentified competing orders are less relevant and that antiferromagnetic spin fluctuations are the dominant feature. Here we report a study of magnetotransport in thin films of the electron-doped copper oxide $\text{La}_{2-x}\text{Ce}_x\text{CuO}_4$. We show that a scattering rate that is linearly dependent on temperature—a key feature of the anomalous normal state properties of the copper oxides—is correlated with the electron pairing. We also show that an envelope of such scattering surrounds the superconducting phase, surviving to zero temperature when superconductivity is suppressed by magnetic fields. Comparison with similar behaviour found in organic superconductors⁵ strongly suggests that the linear dependence on temperature of the resistivity in the electron-doped copper oxides is caused by spin-fluctuation scattering.

Resistivity that increases linearly with temperature (linear-temperature resistivity) is well known to appear in proximity to an antiferromagnetic quantum critical point (QCP), as found in organic⁵ and heavy-fermion⁶ strongly correlated materials. Unlike the hole-doped copper oxides, the absence of anomalous pseudogap physics and other unidentified competing phases in these materials allows such non-Fermi-liquid properties to be attributed to the presence of an antiferromagnetic QCP (ref. 6). This has led to models that ascribe linear-temperature resistivity to a mechanism involving spin fluctuation scattering^{7–9}. The case for this is particularly strong in the Bechgaard class of organic superconductors $(\text{TMTSF})_2\text{PF}_6$, where scattering that increases linearly with temperature (linear-temperature scattering) dominates the normal-state transport above a superconducting state induced by the suppression of a spin-density-wave order by applied pressure⁵. The anisotropic two-dimensional nature of the Bechgaard compounds allows for microscopic calculations of the interdependence of antiferromagnetic and superconducting correlations¹⁰, yielding a thorough understanding of the origin of the anomalous scattering rate in this case^{5,11}. However, in general, no microscopic theory yet exists for the origin of linear-temperature scattering at low temperatures. In $(\text{TMTSF})_2\text{PF}_6$, the linear-temperature scattering rate found at the spin-density-wave QCP has been shown to be suppressed with pressure along with the superconducting transition, with a scattering coefficient that approaches zero along with the transition temperature T_c (refs 5, 11). In electron-doped $\text{Pr}_{2-x}\text{Ce}_x\text{CuO}_4$ (PCCO), linear-temperature resistivity is found down to 35 mK at $x = 0.17$ (ref. 12). Along with other evidence for a Fermi-surface reconstruction^{2,13–15}, this observation suggests that an antiferromagnetic QCP occurs near $x = 0.17$ in PCCO.

$\text{La}_{2-x}\text{Ce}_x\text{CuO}_4$ (LCCO) is an electron-doped copper oxide¹⁶ with properties very similar to PCCO, but with a superconductivity dome

that is slightly shifted towards lower Ce concentrations such that the superconducting phase exists for $0.06 \leq x \leq 0.17$ and is suppressed for $x > 0.17$. The phase diagram of LCCO (Fig. 1), constructed from our

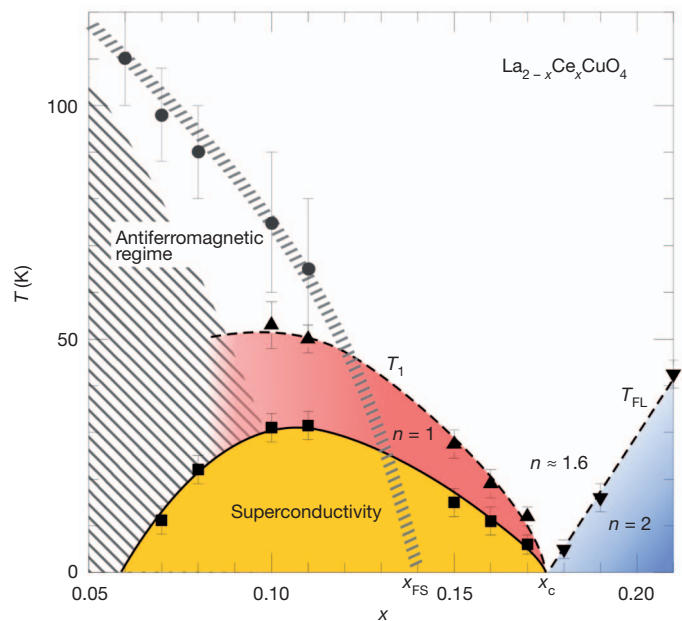


Figure 1 | Temperature-doping (T - x) phase diagram of $\text{La}_{2-x}\text{Ce}_x\text{CuO}_4$. The resistivity in zero field can be expressed by $\rho = \rho_0 + AT^n$, with $n = 1$ and 2 for the red and blue regimes, respectively. Between the $\rho \propto T$ ($n = 1$) and the Fermi-liquid ($n = 2$) regimes, the data below 50 K is well fitted by a single power law with $n \approx 1.6$. The yellow regime is the superconductivity dome. The superconductivity, $\rho \propto T$ and Fermi-liquid regimes terminate at one critical doping, x_c . The temperatures T_1 (triangles) and T_{FL} (inverted triangles) mark the crossover temperatures to the $\rho \propto T$ and Fermi-liquid regimes, respectively. To illustrate the $\rho \propto T$ regime more clearly, the boundary of the superconductivity dome (squares) is defined as the lowest temperature of the linear-temperature resistivity for $x \geq 0.1$. For $x < 0.1$, the resistivity shows an upturn (hatched area) with decreasing temperature, a typical feature of underdoped copper oxides. Owing to the upturn, the superconductivity boundary for $x < 0.1$ is defined as the temperature where the resistivity reaches zero (T_{c0}). The antiferromagnetic (or spin-density-wave) regime (circles) is estimated from previous in-plane angular magnetoresistance measurements¹⁸. A QCP associated with a spin-density-wave Fermi surface reconstruction is estimated to occur near $x = 0.14$ (indicated as x_{FS}). LCCO can only be prepared in thin-film form, so the evidence for a spin-density-wave (antiferromagnetic) QCP under the superconductivity dome is not as conclusive as for the electron-doped copper oxides $\text{Pr}_{2-x}\text{Ce}_x\text{CuO}_4$ or $\text{Nd}_{2-x}\text{Ce}_x\text{CuO}_4$. Nevertheless, in LCCO the change of the sign of the low-temperature Hall coefficient at $x \approx 0.14$ (ref. 19), angular magnetoresistance data, and a low-temperature metal-to-insulator crossover at $x \approx 0.14$ (ref. 16) all suggest that such a QCP, associated with Fermi surface reconstruction, does occur near $x = 0.14$. The error bars on the circles are from ref. 18 and those on other symbols represent the standard error in the fit to the data.

¹Center for Nanophysics & Advanced Materials, University of Maryland, College Park, Maryland 20742, USA. ²Department of Physics, University of Maryland, College Park, Maryland 20742, USA.

present transport studies on optimal to overdoped thin films ($x \geq 0.11$) and prior work^{17–19} for $x < 0.12$, has four distinct regions: the superconducting phase, the linear-temperature ($\rho \propto T$) region, the non-Fermi liquid ($\rho \propto T^{1.6}$) region and the Fermi-liquid ($\rho \propto T^2$) region. In the superconductivity doping range, all films exhibit a linear-temperature resistivity above T_c that extends from T_c up to a characteristic crossover temperature T_1 , forming a shell of anomalous scattering that encases the superconductivity dome. For example, the resistivity of optimally doped $x = 0.11$ is linear from T_c up to $T_1 \approx 45$ K (Supplementary Fig. 1). For higher doping, this temperature range (and thus T_1) decreases, tending towards zero along with T_c itself at the end of the superconductivity dome at a critical doping of $x_c = 0.175 \pm 0.005$. In PCCO, a similar phenomenon is observed (Supplementary Figs 2 and 3) with a linear-temperature region above T_c that extends as far as films can be synthesized (that is, up to $x = 0.19$). Similarly, in hole-doped LSCO ($\text{La}_{2-x}\text{Sr}_x\text{CuO}_4$) a linear-temperature component was shown to diminish upon approaching the end of the doping range of superconductivity²⁰, suggestive of a common relation between scattering and pairing in both electron- and hole-doped copper oxides. The nature of the QCP in hole-doped copper oxides remains uncertain. Note, however, that a linear resistivity identical to that of LSCO (ref. 20) was observed in $\text{La}_{1.6-x}\text{Nd}_{0.4}\text{Sr}_x\text{CuO}_4$ (Nd-LSCO) (ref. 21) at the QCP, where stripe order is known to end.

A direct relation between linear-temperature scattering and T_c is revealed through the doping dependence of each. As shown in Fig. 2, the scattering coefficient $A_1(x)$, obtained from fits to the linear-temperature regions with $\rho(T) = \rho_0 + A_1(x)T$, decreases with T_c as x is increased and approaches zero at the critical doping x_c . This scaling of A_1 with T_c is also observed in PCCO (Supplementary Fig. 4), indicating that it is not specific to the doping concentration (which is

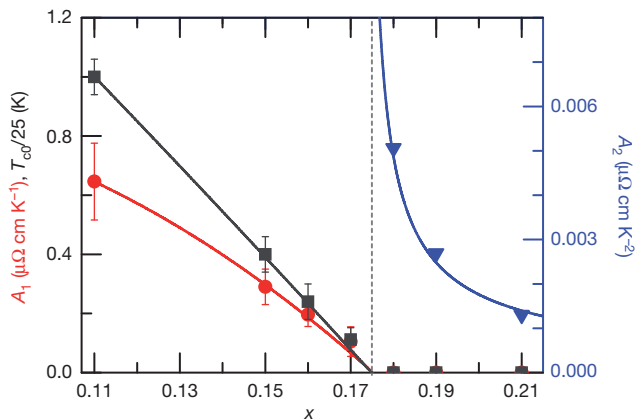


Figure 2 | Doping dependence of scattering rates in zero field. The left vertical axis shows linear-temperature scattering rate A_1 (red circles) and also T_{c0} (divided by 25; black squares) versus x . The right vertical axis shows quadratic scattering rate A_2 (blue triangles) versus x . For the superconducting LCCO films with $x < 0.18$, A_1 data are obtained from the $\rho \propto T$ region ($\rho = \rho_0 + A_1T$, the red regime in Fig. 1). The error bars are the standard deviation over many samples of each doping. We note that in the optimally doped region, the highest superconducting transition temperatures of $x = 0.1$ and 0.11 are almost the same by a slight oxygen variation, and their resistivity also shows similar behaviour. Thus, only one nominal $x = 0.1$ sample was studied here; nevertheless, both the A_1 and T_{c0} (data not shown) fall into the statistical error of the $x = 0.11$ samples. We use the $x = 0.11$ doping to represent the optimal doping level here. For the non-superconducting films with $x \geq 0.18$, A_2 data are obtained from the $\rho \propto T^2$ region ($\rho = \rho_0 + A_2T^2$, the blue regime in Fig. 1). It is noteworthy that the amplitude of the linear-temperature scattering scales with the superconductivity transition temperature (both ending around $x_c = 0.175$), reflecting the intimate relationship between the linear-temperature scattering rate and the superconductivity. From the non-superconductivity side, as the doping approaches x_c from higher doping, the coefficient of electron–electron scattering increases very quickly, reminiscent of critical scattering upon approach to a QCP.

shifted in PCCO compared to LCCO for a given T_c), but is representative of a central relationship between T_c and A_1 . The same relation has been found in $(\text{TMTSF})_2\text{PF}_6$ (refs 5, 11), reflecting the intimate connection between the strength of the linear-temperature inelastic scattering and the electron pairing in systems governed by spin fluctuations. Similar scaling is seen in the hole-doped copper oxides LSCO, Nd-LSCO and $\text{Tl}_2\text{Ba}_2\text{CuO}_{6+\delta}$ (ref. 11), again suggesting that the physics of scattering and pairing is the same in electron- and hole-doped copper oxides.

The linear-temperature scattering is robust and survives in magnetic fields exceeding the upper critical field for superconductivity of LCCO. In fact, when superconductivity is completely suppressed, the linear-temperature resistivity extends down to the $T = 0$ limit without any indication of saturation or change in behaviour. For instance, for $x = 0.15$ at 7.5 T (Fig. 3a, Supplementary Fig. 1), linear-temperature resistivity extends from $T \approx 20$ K down to the lowest measured temperature of 20 mK. Spanning over three decades in temperature, this behaviour clearly points to a scattering mechanism that originates from an anomalous ground state. Similar behaviour is found at higher x (Fig. 3b), but occurs over a decreasing range as T_c is suppressed to zero with doping, again suggesting that linear-temperature scattering is intimately tied to the presence of superconductivity.

Many experiments have shown that spin fluctuations dominate the physical properties in proximity to a critical doping under the superconductivity dome in the more-studied electron-doped copper oxides PCCO and $\text{Nd}_{2-x}\text{Ce}_x\text{CuO}_4$ (refs 2, 22, 23). In analogy with these other electron-doped copper oxides, it is expected that the boundary of antiferromagnetic order in LCCO extrapolates to a QCP beneath the superconductivity dome (indicated as x_{FS} in Fig. 1, where subscript ‘FS’ indicates Fermi surface), having a fundamental role in generating the superconducting phase. In particular, the extended linear-temperature transport scattering that persists to the lowest measurable temperatures is exactly in line with that expected at an antiferromagnetic QCP

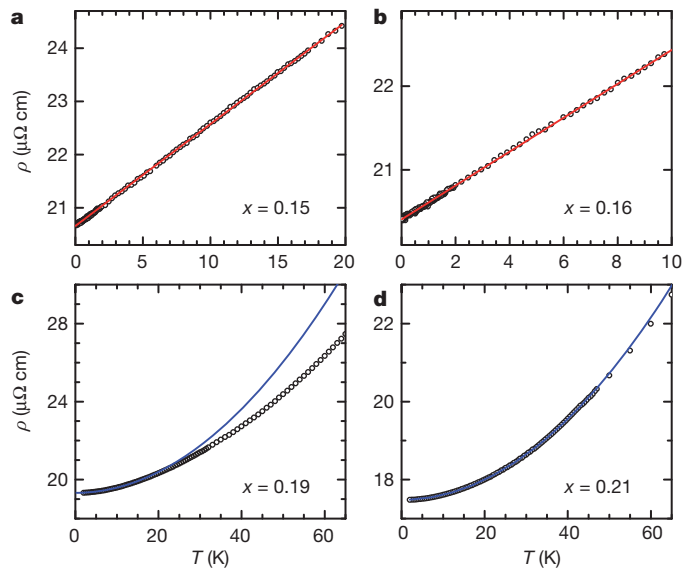


Figure 3 | Temperature dependence of normal-state resistivity. **a** and **b**, $\rho(T)$ of $x = 0.15$ and 0.16 LCCO films in a perpendicular magnetic field where the superconductivity is just suppressed, that is, at 7.5 and 7 T, respectively. The data can be fitted by $\rho = \rho_0 + A_1T$ down to the lowest measuring temperature. The linearity of the resistivity of $x = 0.15$ persists from 20 K down to 20 mK, spanning over three decades in temperature. That is, the $\rho \propto T$ region shown in Fig. 1 can extend down to the $T = 0$ limit, pointing to a scattering mechanism that originates from an anomalous ground state. **c** and **d**, $\rho(T)$ of $x = 0.19$ and 0.21 in zero field, fitted by $\rho = \rho_0 + A_2T^2$ (blue lines). In the non-superconductivity regime ($x \geq 0.18$), the Fermi-liquid behaviour can also persist to the lowest temperature, that is, down to 20 mK (as seen in Supplementary Fig. 5 for $x = 0.18$).

for a two-dimensional disordered Fermi-liquid system⁹. Moreover, inelastic neutron scattering experiments on electron-doped $\text{Pr}_{1-x}\text{La}_x\text{Ce}_x\text{CuO}_{4+\delta}$ show that the strength of the spin fluctuations decreases with overdoping in the superconducting phase and that these fluctuations disappear at the end of the superconductivity dome²⁴.

Non-superconducting films of LCCO doped beyond x_c exhibit a T^2 dependence of $\rho(T)$ in the low-temperature limit, indicating a conventional Fermi-liquid behaviour due to electron-electron scattering, similar to that exhibited by $(\text{TMTSF})_2\text{PF}_6$ (ref. 5) and LSCO (ref. 25). For example, LCCO films with $x = 0.18$ exhibit a T^2 resistivity up to 5 K, spanning over two orders of magnitude in temperature (Supplementary Fig. 5). The highest temperature of the quadratic behaviour (T_{FL} , where subscript FL refers to Fermi liquid) increases with increasing x as shown for $x = 0.19$ and 0.21 (Fig. 3c and d), and notably, this line extrapolates to $T = 0$ at x_c .

In LCCO, the critical doping x_c is exactly where the superconductivity dome terminates and the two characteristic crossover temperatures T_1 and T_{FL} approach absolute zero. Interestingly, indications of the singular nature of x_c are evident even from within the overdoped Fermi liquid regime of LCCO. In this region of the phase diagram, the coefficient of electron-electron scattering $A_2(x)$ (that is, obtained from fits to $\rho(T) = \rho_0 + A_2(x)T^2$) exhibits a strong enhancement upon approach to x_c from higher doping, reminiscent of critical scattering upon approach to a QCP (ref. 6). This suggests that the onset of superconductivity marks a dramatic change in the ground state and its excitations. While Fermi-liquid behaviour of resistivity has been reported at one doping in both hole-doped LSCO (ref. 25) and $\text{Ti}_2\text{Ba}_2\text{CuO}_{6+\delta}$ (ref. 26), such doping-tuned critical behaviour in the non-superconducting region was not observed. In LCCO, the resistivity directly above the critical point at $x = 0.175$ and in the entire temperature regime above the characteristic temperatures T_1 and T_{FL} is best fitted by a single power-law dependence, $\rho = \rho_0 + A'T^n$ with $n \approx 1.6$, up to at least 50 K (Supplementary Fig. 6). Perhaps not coincidentally, the same power law is observed above the Fermi-liquid ($\propto T^2$) regime in LSCO (refs 20, 25), signifying that scattering throughout the non-Fermi-liquid regime is governed by the same physics in both hole- and electron-doped copper oxides. Clearly, our observation of critical behaviour at x_c will require further experimental and theoretical investigation to determine its significance for the unusual transport properties of the copper oxides.

With the absence of anomalous pseudogap phenomena in electron-doped copper oxides², comparisons to similarly tractable systems allow for far-reaching conclusions to be drawn. Studies^{5,10,11} of the organic superconductor $(\text{TMTSF})_2\text{PF}_6$ show that electron pairing and linear-temperature scattering arise from antiferromagnetic (spin-density-wave) spin fluctuations. Given the very similar experimental transport properties and evolution of ground states in the phase diagram of LCCO, it is likely that the scattering and pairing in the electron-doped copper oxides is governed by a similar interplay of spin fluctuations and superconductivity. The results of our work reported here, and their analogy to $(\text{TMTSF})_2\text{PF}_6$, strongly suggests that the pairing in electron-doped copper oxides is not coming from phonons or any other unusual pseudogap order parameter (such as d -density waves, orbital currents or stripe order), but rather from spin-fluctuation-mediated pairing^{27–29}. The striking similarities between transport properties of electron- and hole-doped copper oxides provides evidence that the mechanism of the anomalous linear-temperature scattering rate and high- T_c pairing are shared between the two families, and, furthermore, bear a striking resemblance to simpler systems well described by the spin fluctuation scenario. Although the role of the pseudogap and unidentified competing phases in the hole-doped copper oxides remains to be conclusively determined, the similar correlation between the linear-temperature scattering and T_c for both electron- and hole-doped copper oxides suggests that spin fluctuations also play a crucial part in hole-doped copper oxides.

Received 4 March; accepted 15 June 2011.

1. Norman, M. R. The challenge of unconventional superconductivity. *Science* **332**, 196–200 (2011).
2. Armitage, N. P., Fournier, P. & Greene, R. L. Progress and perspectives on the electron-doped cuprates. *Rev. Mod. Phys.* **82**, 2421–2487 (2010).
3. Weber, C., Haule, K. & Kotliar, G. Strength of correlations in electron- and hole-doped cuprates. *Nature Phys.* **6**, 574–578 (2010).
4. Senechal, D. & Tremblay, A.-M. S. Hot spots and pseudogaps for hole- and electron-doped high-temperature superconductors. *Phys. Rev. Lett.* **92**, 126401 (2004).
5. Doiron-Leyraud, N. *et al.* Correlation between linear resistivity and T_c in the Bechgaard salts and the pnictide superconductor $\text{Ba}(\text{Fe}_{1-x}\text{Co}_x)_2\text{As}_2$. *Phys. Rev. B* **80**, 214531 (2009).
6. Löhneysen, H., v., Rosch, A., Vojta, M. & Wölfle, P. Fermi-liquid instabilities at magnetic quantum phase transitions. *Rev. Mod. Phys.* **79**, 1015–1075 (2007).
7. Moriya, T. & Ueda, K. Spin fluctuations and high temperature superconductivity. *Adv. Phys.* **49**, 555–606 (2000).
8. Sachdev, S. & Keimer, B. Quantum criticality. *Phys. Today* **64**, 29–35 (2011).
9. Rosch, A. Magnetotransport in nearly antiferromagnetic metals. *Phys. Rev. B* **62**, 4945–4962 (2000).
10. Bourbonnais, C. & Sedeki, A. Link between antiferromagnetism and superconductivity probed by nuclear spin relaxation in organic conductors. *Phys. Rev. B* **80**, 085105 (2009).
11. Taillefer, L. Scattering and pairing in cuprate superconductors. *Annu. Rev. Cond. Matter Phys.* **1**, 51–70 (2010).
12. Fournier, P. *et al.* Insulator-metal crossover near optimal doping in $\text{Pr}_{2-x}\text{Ce}_x\text{CuO}_4$: Anomalous normal-state low temperature resistivity. *Phys. Rev. Lett.* **81**, 4720–4723 (1998).
13. Dagan, Y. *et al.* Evidence for a quantum phase transition in $\text{Pr}_{2-x}\text{Ce}_x\text{CuO}_{4-\delta}$. *Phys. Rev. Lett.* **92**, 167001 (2004).
14. Matsui, H. *et al.* Evolution of the pseudogap across the magnet-superconductor phase boundary of $\text{Nd}_{2-x}\text{Ce}_x\text{CuO}_4$. *Phys. Rev. B* **75**, 224514 (2007).
15. Helm, T. *et al.* Evolution of the Fermi surface of the electron-doped high-temperature superconductor $\text{Nd}_{2-x}\text{Ce}_x\text{CuO}_4$ revealed by Shubnikov-de Haas oscillations. *Phys. Rev. Lett.* **103**, 157002 (2009).
16. Sawa, A. *et al.* Electron-doped superconductor $\text{La}_{2-x}\text{Ce}_x\text{CuO}_4$: preparation of thin films and modified doping range for superconductivity. *Phys. Rev. B* **66**, 014531 (2002).
17. Jin, K. *et al.* Normal-state transport in electron-doped $\text{La}_{2-x}\text{Ce}_x\text{CuO}_4$ thin films in magnetic fields up to 40 Tesla. *Phys. Rev. B* **77**, 172503 (2008).
18. Jin, K. *et al.* Evidence for antiferromagnetic order in $\text{La}_{2-x}\text{Ce}_x\text{CuO}_4$ from angular magnetoresistance measurements. *Phys. Rev. B* **80**, 012501 (2009).
19. Jin, K. *et al.* Low-temperature Hall effect in electron-doped superconducting $\text{La}_{2-x}\text{Ce}_x\text{CuO}_4$ thin films. *Phys. Rev. B* **78**, 174521 (2008).
20. Cooper, R. A. *et al.* Anomalous criticality in the electrical resistivity of $\text{La}_{2-x}\text{Sr}_x\text{CuO}_4$. *Science* **323**, 603–607 (2009).
21. Daou, R. *et al.* Linear temperature dependence of resistivity and change in the Fermi surface at the pseudogap critical point of a high- T_c superconductor. *Nature Phys.* **5**, 31–34 (2009).
22. Motoyama, E. M. *et al.* Spin correlations in the electron-doped high-transition-temperature superconductor $\text{Nd}_{2-x}\text{Ce}_x\text{CuO}_{4\pm\delta}$. *Nature* **445**, 186–189 (2007).
23. Lin, J. & Millis, A. J. Theory of low-temperature Hall effect in electron-doped cuprates. *Phys. Rev. B* **72**, 214506 (2005).
24. Fujita, M. *et al.* Low-energy spin fluctuations in the ground states of electron-doped $\text{Pr}_{1-x}\text{La}_x\text{Ce}_x\text{CuO}_{4+\delta}$ cuprate superconductors. *Phys. Rev. Lett.* **101**, 107003 (2008).
25. Nakamae, S. *et al.* Electronic ground state of heavily overdoped nonsuperconducting $\text{La}_{2-x}\text{Sr}_x\text{CuO}_4$. *Phys. Rev. B* **68**, 100502 (2003).
26. Kubo, Y., Shimakawa, Y., Manako, T. & Igarashi, H. Transport and magnetic properties of $\text{Ti}_2\text{Ba}_2\text{CuO}_{6+\delta}$ showing a δ -dependent gradual transition from an 85-K superconductor to a nonsuperconducting metal. *Phys. Rev. B* **43**, 7875–7882 (1991).
27. Scalapino, D. J. The case for $d_{x^2-y^2}$ pairing in the cuprate superconductors. *Phys. Rep.* **250**, 329–365 (1995).
28. Dhokarh, D. D. & Chubukov, A. V. Self-consistent Eliashberg theory, T_c , and the gap function in electron-doped cuprates. *Phys. Rev. B* **83**, 064518 (2011).
29. Monthoux, P., Pines, D. & Lonzarich, G. G. Superconductivity without phonons. *Nature* **450**, 1177–1183 (2007).

Supplementary Information is linked to the online version of the paper at www.nature.com/nature.

Acknowledgements We thank L. Taillefer for extensive discussions and N. Doiron-Leyraud for some preliminary analysis of our zero-field data. We also appreciate discussions with A. Chubukov, A. Millis and C. Varma. Some experimental help was provided by X. Zhang, P. Bach and G. Droulers. This research was supported by the NSF under DMR-0952716 (J.P. and K.K.) and DMR-0653535 (R.L.G.) and the Maryland Center for Nanophysics and Advanced Materials (K.J. and N.P.B.).

Author Contributions K.J. prepared and characterized the thin-film samples. K.J., N.P.B., K.K. and J.P. performed the transport measurements and data analysis. N.P.B., J.P. and R.L.G. wrote the manuscript. R.L.G. conceived and directed the project.

Author Information Reprints and permissions information is available at www.nature.com/reprints. The authors declare no competing financial interests. Readers are welcome to comment on the online version of this article at www.nature.com/nature. Correspondence and requests for materials should be addressed to R.L.G. (rgreene@squid.umd.edu).

Samples. The c-axis-oriented $\text{La}_{2-x}\text{Ce}_x\text{CuO}_4$ (LCCO) and $\text{Pr}_{2-x}\text{Ce}_x\text{CuO}_4$ (PCCO) films were deposited directly on (100) SrTiO_3 substrates by a pulsed laser deposition (PLD) technique utilizing a KrF excimer laser as the exciting light source¹⁸. The films were typically 100-150 nm in thickness. Since the oxygen content has an influence on both the superconducting and normal state properties of the material¹³, we took extra care in optimizing the annealing process for each Ce concentration. We prepared many films with variable oxygen content, and found that the optimized samples showed metallic behavior down to the lowest measured temperature (20 mK), while non-optimized samples often show an upturn (either in fields or at zero field) at low T , due to oxygen-induced disorders. Moreover, the optimized samples showed a narrow transition width (for superconducting samples) and low residual resistivity (for nonsuperconducting samples). Using these criteria, we found the best film growth conditions and excellent reproducibility of the transport data presented here. The films were patterned into Hall bar bridges using photolithography and ion milling techniques for the transport measurements.

Measurements. The high- T measurements (above 2 K) were carried out in a 14T PPMS and low- T measurements were done in an Oxford dilution fridge (down to 20 mK), with an overlapped temperature range. For example, the linear-in- T resistivity data shown in Fig. 3a were measured in the dilution fridge from 20 mK to 20 K. Electrical current was applied in the ab-plane while the magnetic field was applied along the c-axis.

The boundary of the superconducting dome. The boundaries of superconductivity for both LCCO (Fig. 1) and PCCO (Fig. S3) are determined as the temperature at which the resistivity starts to deviate from the linear-in- T resistivity behavior as seen in Figures S1 and S2, respectively. For the underdoped samples, since there is an upturn of the resistivity above the superconducting transition, we define the zero resistive state temperature (T_{c0}) as the superconducting boundary.

Universal relation between A_1 and T_c for PCCO and LCCO. A comparison between PCCO and LCCO shows that the A_1 to T_c scaling is a universal behavior in electron-doped copper oxides. Because of the different optimal doping levels, we normalize the $A_1(x)$ to the coefficient at the optimal doping, i.e., $A_{\text{opt}} = A_1(x = 0.15)$ for PCCO and $= A_1(x = 0.11)$ for LCCO. The x axes are plotted with the same interval ($\Delta x = 0.01$) but with different starting points ($x = 0.15$ for PCCO and $= 0.11$ for LCCO) for the comparison shown in Fig. S4. The doping dependence of the normalized coefficient data ($A_1(x)/A_{\text{opt}}$) of PCCO and LCCO fall onto one straight line, suggesting the linear resistivity in PCCO would disappear at a doping $x \sim 0.215$. The normalized superconducting transition temperature ($T_c(x)/T_c^{\text{opt}}$) also falls onto one straight line. That is, the superconducting transition temperature scales with the coefficient of the linear term, reflecting the intimate relation between the strength of the linear resistivity and the electron pairing. We note that the $A_1(x)/A_{\text{opt}}$ scales monotonically with $T_c(x)/T_c^{\text{opt}}$ in the overdoped region, but a maximum is found between $x = 0.16$ and 0.17 for PCCO (see Fig. S4b). This change is most likely associated with the Fermi surface reconstruction quantum critical point (QCP) found at this doping¹³⁻¹⁵. Below this QCP, the low T resistivity starts to have an upturn, which also adversely impacts the coefficient of any attempted linear fit. This is also true for LCCO (ref. 16). In LCCO, the normalized $A_1(x)$ values suggest that an analogous QCP would exist between $x = 0.12$ and $x = 0.14$, which is consistent with the extrapolated antiferromagnetic (spin density wave) endpoint in the phase diagram (Fig. 1).

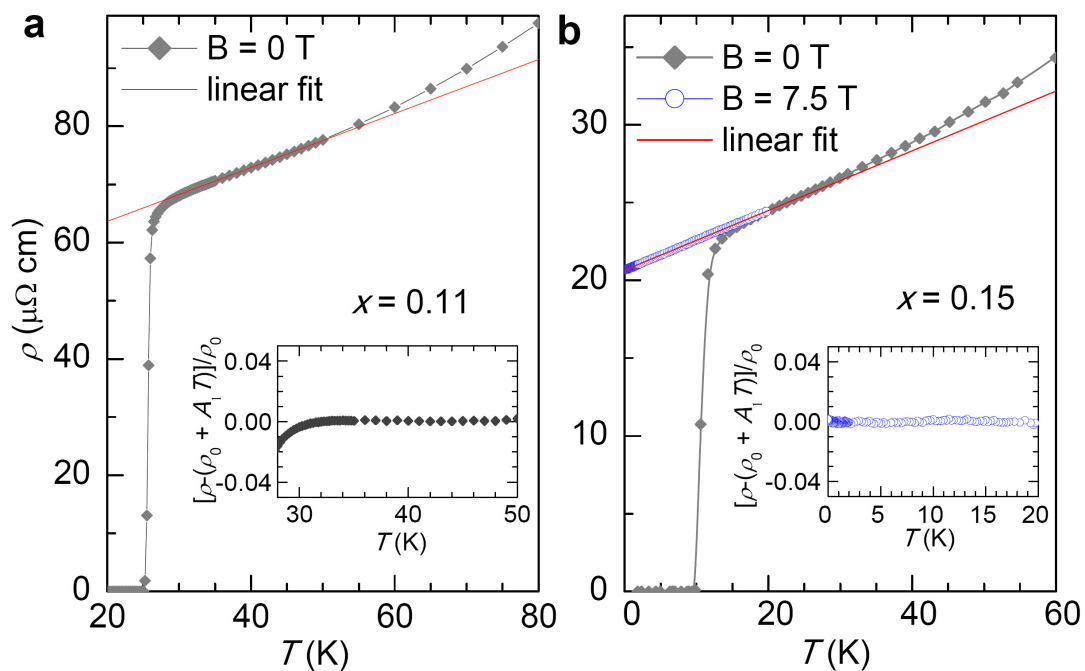


Figure S1 | Temperature dependence of resistivity in superconducting $\text{La}_{2-x}\text{Ce}_x\text{CuO}_4$ (LCCO). **a**, $\rho(T)$ of optimally doped LCCO with $x = 0.11$ in zero field (diamonds), fitted by $\rho(T) = \rho_0 + A_1 T$ (red line). **b**, $\rho(T)$ of $x = 0.15$ at 0 (diamonds) and 7.5 T (circles). The red line is the linear fit to the 7.5 T data. The insets show the fitting quality presented as $\Delta\rho/\rho$ vs. T , where $\Delta\rho = \rho - (\rho_0 + A_1 T)$.

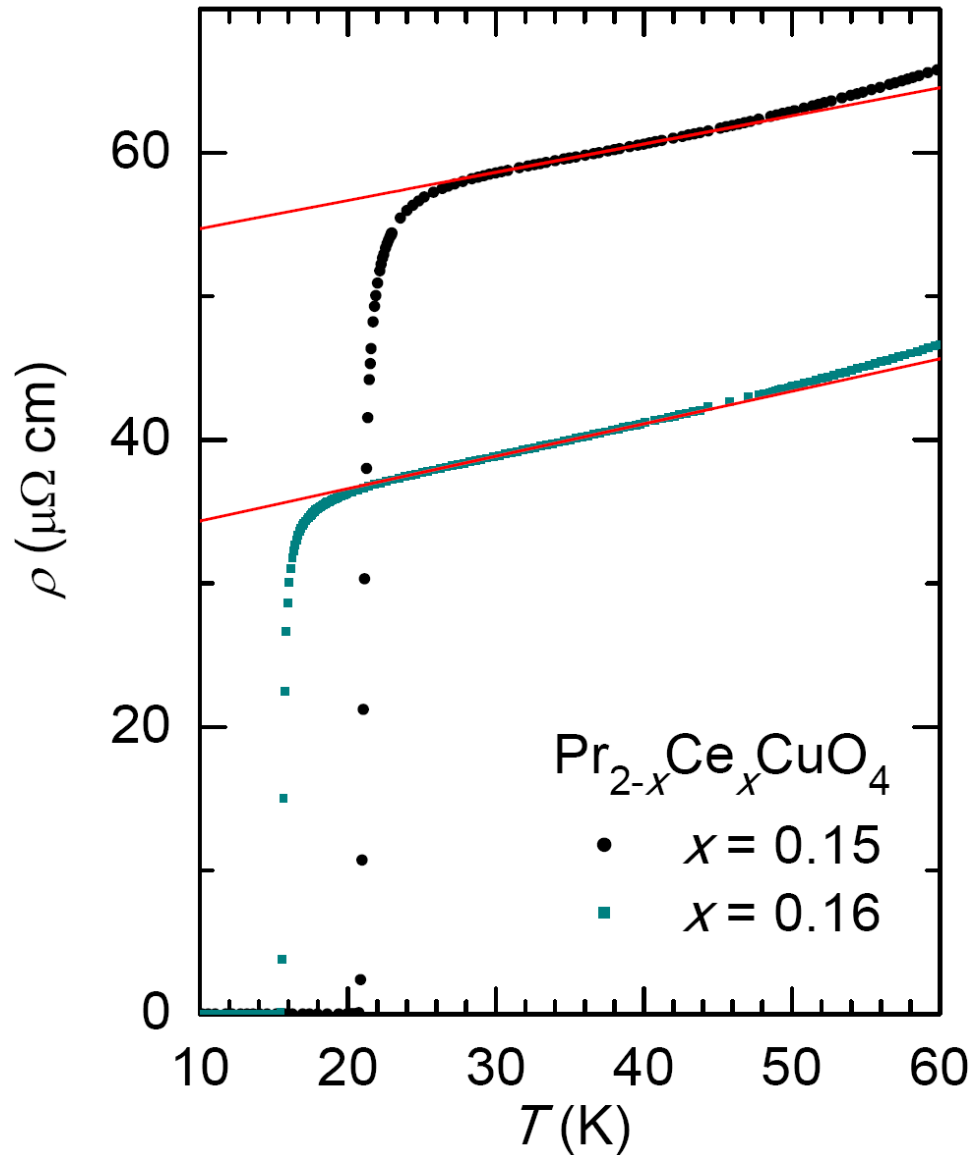


Figure S2 | Linear-in-temperature dependence of resistivity in superconducting $\text{Pr}_{2-x}\text{Ce}_x\text{CuO}_4$ (PCCO) films. $\rho(T)$ of PCCO with $x = 0.15$ and 0.16 in zero field, fitted by $\rho(T) = \rho_0 + A_1T$ (red lines). The data are from ref. 13.

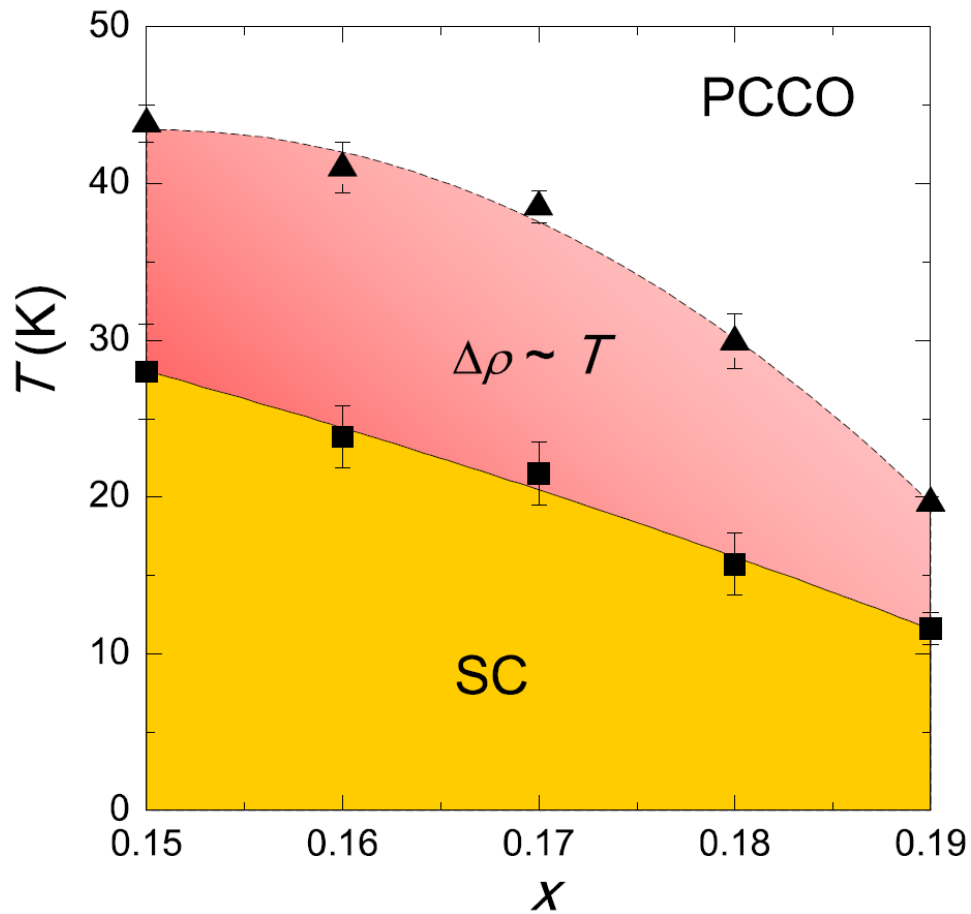


Figure S3 | Temperature-doping (T, x) phase diagram of PCCO in zero field.

The phase diagram of PCCO with $0.15 \leq x \leq 0.19$ shows superconducting (SC) and T -linear regions. The boundaries of SC and T -linear regions are defined as the starting and ending temperatures of the T -linear resistivity (see Fig. S2). Error bars represent the standard error in the fit.

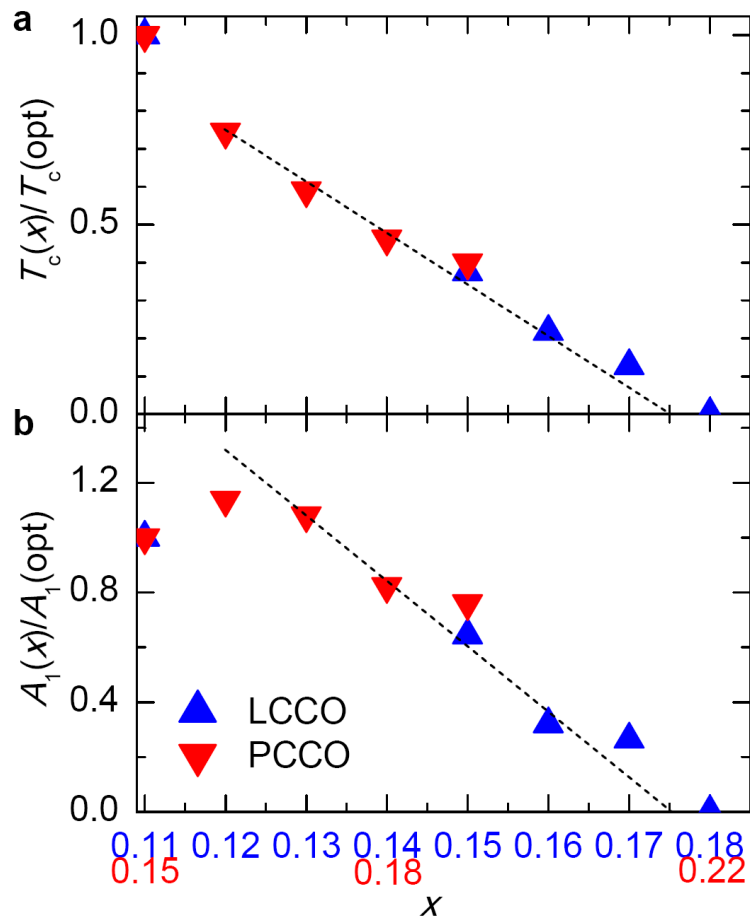


Figure S4 | Relation between the superconducting transition temperature and the scattering rate in LCCO and PCCO. **a**, Doping dependence of reduced T_c , is normalized to the superconducting transition temperature of the optimal doping at $x = 0.11$ and 0.15 for LCCO and PCCO, respectively. **b**, Doping dependence of reduced $A_1(x)$ (normalized to that of optimal doping), the coefficient of the linear resistivity in $\rho \propto T$ regime. The x axes for LCCO and PCCO start from their optimal doping levels, $x = 0.11$ and 0.15 , respectively (see text for details).

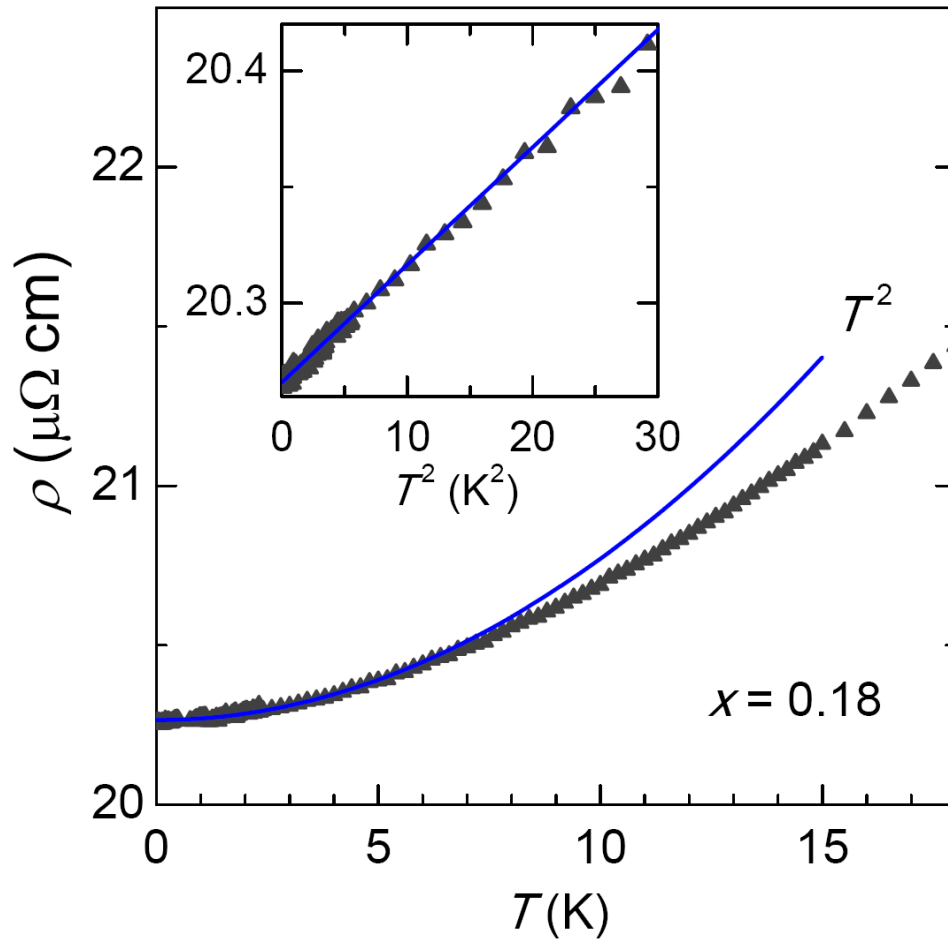


Figure S5 | Temperature dependence of resistivity in LCCO with $x = 0.18$. ρ (T) of $x = 0.18$ in zero field (triangles), fitted by $\rho(T) = \rho_0 + A_2T^2$ (blue line). The resistivity shows a Fermi liquid behavior from 20 mK to ~ 5 K. Inset: ρ (T) versus T^2 in the Fermi liquid range.

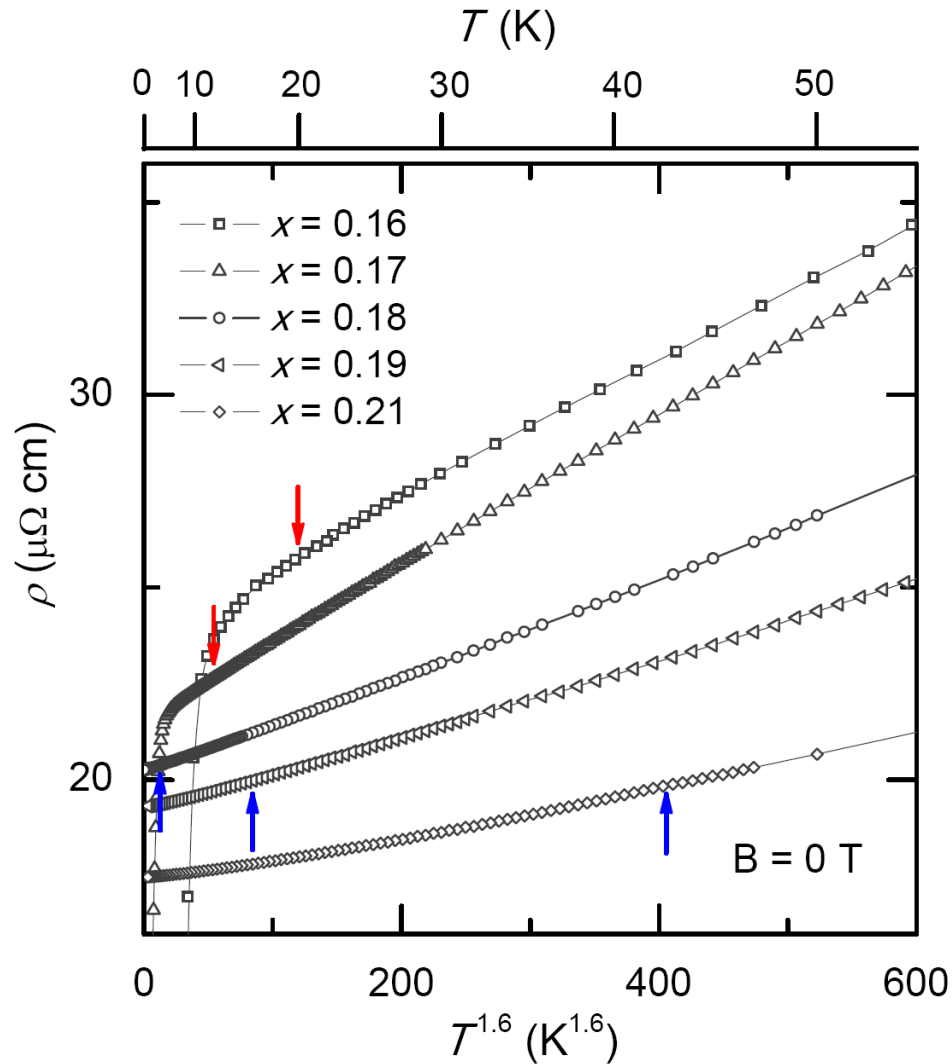


Figure S6 | Temperature dependence of resistivity in LCCO from $x = 0.16$ to 0.21 . $\rho(T)$ of $x = 0.16, 0.17, 0.18, 0.19,$ and 0.21 in zero field (symbols), plotted against $T^{1.6}$. All these doping levels show an approximate behavior, $\rho \propto T^{1.6}$ somewhat above the crossover temperatures, T_1 (red arrows) and T_{FL} (blue arrows). For clarity, we also put a linear scale of temperature on the top.